Ultrasonic guided waves on a periodical grating : coupled modes in the first Brillouin zone

B. Morvan, Anne-Christine Hladky, D. Leduc, J.L. Izbicki

Ultrasonic guided waves on a periodical grating: Coupled modes in the first Brillouin zone

Cite as: J. Appl. Phys. **101**, 114906 (2007); https://doi.org/10.1063/1.2737348
Submitted: 17 January 2007 • Accepted: 31 March 2007 • Published Online: 05 June 2007

Bruno Morvan, Anne-Christine Hladky-Hennion, Damien Leduc, et al.

Ultrasonic guided waves on a periodical grating: Coupled modes in the first Brillouin zone

Bruno Morvan[a)]
Laboratoire d'Acoustique Ultrasonore et d'Electronique, UMR CNRS 6068, Université du Havre, Place Robert Schuman, Boîte Postale 4006, 76610 Le Havre, France

Anne-Christine Hladky-Hennion
Institut d'Electronique, de Microélectronique et de Nanotechnologie, UMR CNRS 8520, 41 boulevard Vauban, 59046 Lille, France

Damien Leduc and Jean-Louis Izbicki
Laboratoire d'Acoustique Ultrasonore et d'Electronique, UMR CNRS 6068, Université du Havre, Place Robert Schuman, Boîte Postale 4006, 76610 Le Havre, France

(Received 17 January 2007; accepted 31 March 2007; published online 5 June 2007)

The propagation of Lamb waves in a plate with an engraved periodic grating is addressed in this article. Mode conversions and reflections are analyzed. In the first part the conversion modes are explained by the existence of a resonance condition between the Lamb-wave wavenumbers and the fundamental and harmonic spatial periods of the grating. These phenomena are experimentally and numerically highlighted for a metallic waveguide with a rectangular grating. The second part focuses on the pseudo-Lamb wave dispersion curves in a periodic waveguide. The periodicity implies that the Lamb waves dispersion curves fold back at the edge of the Brillouin zone. Several stop bands appear: classical band gaps at the boundary of the Brillouin zone and mini-stop-bands inside the Brillouin zone. For the ministop band, dispersion curves cross and a possible coupling occurs between the modes. Finally, conversions or the existence of gaps are linked with the Power Spectral Density of the grating profile. © *2007 American Institute of Physics*.
[DOI: 10.1063/1.2737348]

I. INTRODUCTION

Lamb waves are of great interest in the nondestructive evaluation of surfaces or interfaces. The particular case of periodic surfaces is studied in this article. Understanding this problem can be useful, for example, to evaluate ribbed plate or sandwich panels utilizing a honeycomb core. It was shown that a guided wave is attenuated when propagating on a plate with a rough surface.[1–4] The amplitude attenuation is related to the Root Mean Square (RMS) value of the depth of the roughness. Potel *et al.*[4] have shown the importance of the spatial periods of the surface for the calculation of the attenuation. Furthermore, attenuation depends on the considered Lamb mode. An original approach to the problem consists in interpreting the attenuation by an energy transfer between modes.[5] This approach also supposes restriction on the value of the rms and a weak variation of the surface profile. Therefore, in the presence of roughness, an incident propagating mode is converted in propagating or localized modes. Consequently, the energy lost by the incident wave is divided among a wide number of modes.

If the plate is periodically corrugated, mode coupling involves interference processes. In this case, a phase matching between the incident and one special converted mode can occur. This phenomenon has been extensively studied in the case of the propagation of sound waves in a waveguide with sinusoidally perturbed rigid wall.[6–8] Some other recent works deal with the propagation of Lamb waves in an elastic plate having periodically corrugated free surfaces.[9–13] El Bahrawy[9] shows by using a modal approach that inside a stopband a Lamb mode can interact with another Lamb mode. This interaction leads to crossover point in the Lamb waves dispersion curves. This phenomenon was experimentally studied by Leduc *et al.* in Ref. 13 in the case of an incident wave propagating in a plate with a surface grating composed by triangular grooves. It is shown that converted reflected waves are observed depending on the period of the corrugated surface.

The case of a multiperiodic surface has been studied theoretically by means of the multiscale method.[14] The number of possibilities to have different coupled modes increases and then wider stop bands can be obtained. In this paper, it is shown that for a rectangular grating there is an interaction between an incident Lamb wave with the fundamental period of the grating and also with the spatial harmonic components. In the first part, we present a transient analysis of Lamb wave propagation on a corrugated plate by a Finite Element Method. Two rectangular geometries are studied and particularly the effect of the shape of the rectangular corrugation. In the second part, an experimental study is performed on the same plates.

In the last part, interpretation of the conversion phenomena is done by considering the dispersion curves of the propagating modes in a plate with an infinite periodical surface grating. The dispersion curves exhibit a folding effect and band gaps. Some band gaps inside the first Brillouin

[a)]Electronic mail: bruno.morvan@univ-lehavre.fr

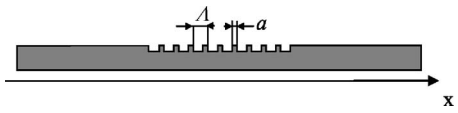

FIG. 1. Geometry of the studied samples. Λ is the periodicity and a is the length of the higher part of the pattern. x is the direction of propagation.

zone appear at particular dispersion curves crossing. It is shown that these "mini-stop bands" exist for the frequencies where converted waves were previously observed.

II. POSITION OF THE PROBLEM

The geometry of the studied corrugated plate is shown in Fig. 1. Λ is the periodicity and a is the length of the higher part of the pattern. Two specimens are considered: a rectangular surface grating with a ratio $a/\Lambda=1/3$ and a square surface grating such that $a/\Lambda=1/2$. The period of the grating Λ is equal to 6 mm. The thickness of the aluminum plates is 5 mm whereas the corrugation depth is equal to 100 μm. Concerning the Lamb wave propagation, the corrugation can then be treated as a small perturbation.

The power spectral density (PSD) of the two profiles is drawn in Figs. 2(a) and 2(b). It is obtained by the Fourier transform of the autocovariance function calculated from the surface profile. It gives the spatial wavelength components of the surface. It was already pointed out that an incident Lamb mode can interact with the wavenumber of the surface corrugation. In a previous study[11] authors have shown that the interaction of the incident wave with the grating can be reduced to a relation between the wave vectors

$$\mathbf{k}_{\text{inc}} - \mathbf{k}_{\text{conv}} = \mathbf{G} \tag{1}$$

where $\mathbf{G}$ is one vector of the reciprocal lattice (by analogy with the crystalline structures). $\mathbf{G}$ is defined by: $\mathbf{G}=(2\pi/\Lambda)\mathbf{u}x$. $\mathbf{k}_{\text{inc}}$ and $\mathbf{k}_{\text{conv}}$ are, respectively, the wave vectors of the incident and reflected converted waves. It should be noted that the incident and the converted modes can be

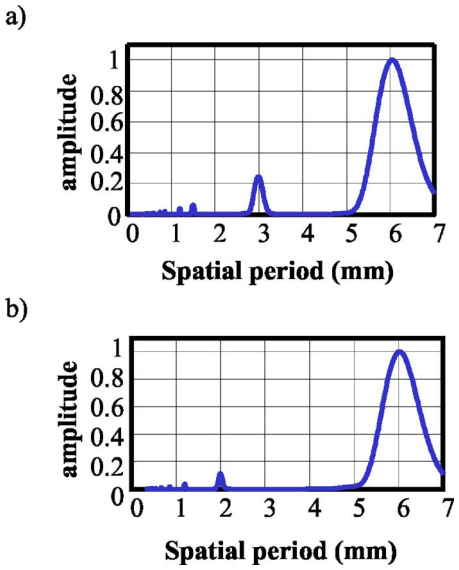

FIG. 2. Power Spectral Density of the surface profile of the studied samples against the spatial period Λ. (a) Rectangular grating and (b) square grating.

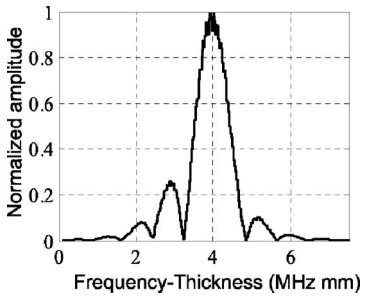

FIG. 3. FEM study. Amplitude of the S_0 incident wave vs frequency-thickness product.

either codirectional or contradirectional. Relation (1) restricts the interaction of the incident wave to the fundamental grating period. The converted waves excited on two successive grooves must be in phase and the phase matching corresponds to the smaller path. Whatever the path the general condition is

$$\mathbf{k}_{\text{inc}} - \mathbf{k}_{\text{conv}} = n\mathbf{G}, \tag{2}$$

where n is an integer. Therefore, incident and converted wavelengths are also coupled to the harmonics of the grating (Λ/n).

We are interested in the interaction of a Lamb wave with the harmonic components (wave vector $n\cdot k_\Lambda$). This is necessary to use the fact that the PSD of the profile contains Λ/n harmonics. The interaction will be enhanced if the amplitude of these harmonics is strong. Therefore, it is interesting to study a rectangular profile instead of a triangular profile used in the previous study.[11] Moreover, the variation of this amplitude can be controlled by the antisymmetric shape of the rectangular profile.

III. NUMERICAL PROCESSING

The numerical study is performed with the ATILA® code.[15] The two-dimensional (2D) model is a 200 mm long plate with a limited grating on one side (Fig. 1). The acoustics parameters, longitudinal and shear velocities, are, respectively, $c_L=6350$ m/s and $c_T=3100$ m/s. The density of the aluminum is equal to 2700 kg/m^3. Only a part of one side is engraved with eleven identical rectangular grooves. The surface is flat before and after the grating: it enables to generate and identify the incident Lamb mode. A transient analysis is performed. A single mode is generated at the first extremity of the plate by imposing its corresponding theoretical displacements in the thickness. The excitation is quasiharmonic and limited to five periods. The transient analysis allows us to follow the propagation of this mode in the space-time domain and particularly its interaction with the grating. The normal surface displacements are calculated. From these displacements, the identification of the propagating modes is performed in the dual space by applying a time and a spatial fast Fourier transform (2D FFT).

The incident wave (positive wave number) is the fundamental symmetrical wave S_0, generated on a frequency bandwidth centered at $f=800$ kHz, corresponding to a frequency-thickness product equal to 4 MHz·mm. In Fig. 3 the amplitude of the S_0 mode versus frequency is plotted. The

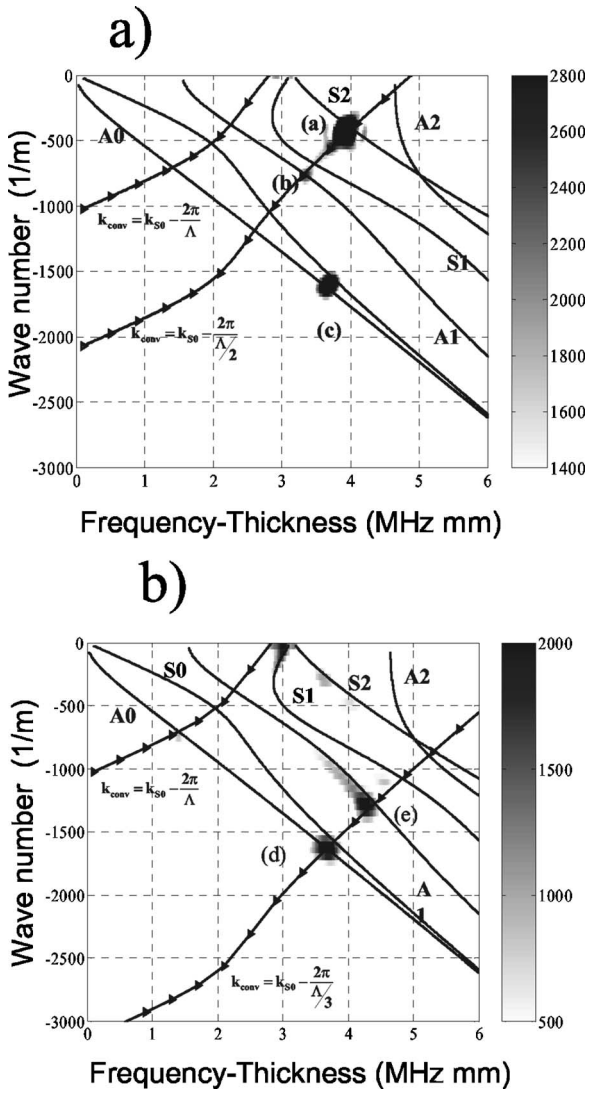

FIG. 4. FEM study. Incident S_0 wave. Identification of the converted/reflected waves in the wave number/frequency space. The theoretical dispersion curves are plotted in solid line. The solid lines with triangle represent the wave numbers $\mathbf{k}_{conv}$ obtain by relation (2) $\mathbf{k}_{inc}=\mathbf{k}_{S_0}$. (a) Rectangular grating and (b) square grating.

bandwidth of the signal [approximately (3.6–4.4 MHz mm)] is due to the short time duration of the tone burst. We are interested in mode conversions under the grating. Five modes can propagate (A_0, S_0, A_1, S_1, and S_2) in the considered frequency range (Fig. 4). A 2D FFT of the different time-space signals on each sample enables to identify the converted modes. In the case of the rectangular grating [Fig. 4(a)], reflected Lamb mode S_2 is observed with a very strong amplitude at $f=4$ MHz mm [spot (a)]. A_1 mode at $f=3.35$ MHz mm [spot (b)] and A_0 or S_0 at $f=3.65$ MHz mm [spot (c)] are also present. From relation (1), the wavevector of the converted waves can be calculated. The curves describing the evolution of the wavenumbers k_{conv} versus frequency are represented in solid line with triangle in Fig. 4. Each intersection of these curves with a Lamb wave dispersion curves indicates a possible conversion of the incident wave. In Fig. 2(b), the PSD of the profile shows that the harmonic 2 is present. Indeed conversions into reflected waves are observed and the wave vectors of

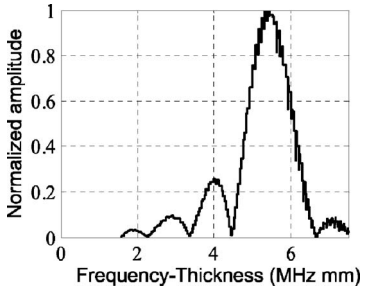

FIG. 5. FEM study. Amplitude of the A_1 incident wave vs frequency-thickness product.

these waves check the Eq. (2) with $N=2$. The reflected wave, identified by the spot (c) on the Fig. 4(a) cannot be explained by relation (2). At this frequency, the wavelength of the incident mode is equal to 4 mm and this length is equal to (A-*a*) (Fig. 1). We can formulate the hypothesis that a S_0 standing wave is present in each groove of the grating.

The square profile has only odd harmonics. The signals in the wave number/frequency space show that conversions related to the harmonic 2 disappear whereas conversions related to the harmonic 3 appear $[k_{conv}=k_{S_0}-2\pi/(\Lambda/3)]$. A_0 and A_1 Lamb waves are observed for frequency-thickness products equal, respectively, to 3.65 and 4.3 MHz mm [spots (d) and (e)].

The same study is repeated with the incident A_1 wave excited at the frequency-thickness 5.5 MHz mm (Fig. 5). Figures 6(a) and 6(b) give, respectively, the converted reflected waves in the case of the rectangular and square grating. The theoretical values k_{conv} from Eq. (2) are superimposed to the 2D FFT representation of signals. In the case of the rectangular surface profile, only converted modes associated to the fundamental period and to the even harmonics ($N=2$ and $N=4$) are present in accordance with the spectral content of the PSD (Fig. 2). The case of the spot (f) corresponding to a converted reflected S_1 wave is quite different. At this frequency, three modes are coupled: A_1, A_0, and S_1 modes. Indeed A_1 is converted in the A_0 reflected wave $[k_{A_0}=k_{A_1}-2\pi/(\Lambda/4)]$ due to the presence of the fourth harmonic in the PSD. Then, in his turn, the A_0 reflected mode is itself converted in an S_1 wave propagating in the same negative x direction ($k_{S_1}=-k_{A_0}-2\pi/\Lambda$). The case of the coupling between three modes in a two-dimensional multiperiodic waveguide was also studied by Asfar.[12]

The interaction of the incident A_1 Lamb wave with the square grating is shown in Fig. 6(b). Only converted modes coupled to the odd harmonics of the grating are excited. The indirect conversion in the A_0 Lamb wave at frequency $fe=1.07$ MHz mm is observed [spot (g)]. At this frequency the incident A_1 mode and reflected A_0 and S_1 modes are coupled.

IV. EXPERIMENTAL VERIFICATION

Two corrugated plates are studied (experimentally) with, respectively, a square and rectangular grating. The studied plates are engraved with 11 rectangular grooves and the surface profiles are identical to those considered with the finite element method (Fig. 1). Plate thicknesses are 4.75 and 4.45 mm for, respectively, the square and rectangular plates. A

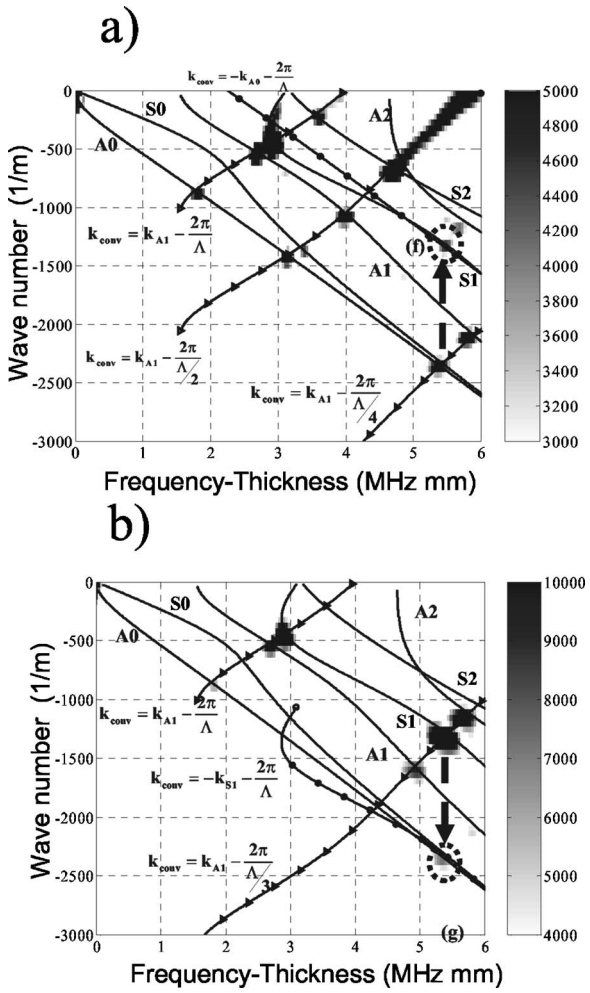

FIG. 6. FEM study. Incident A_1 wave. Identification of the converted/reflected waves in the wavenumber/frequency space. The theoretical dispersion curves are plotted in solid line. The solid lines with triangle represent the wavenumbers $\mathbf{k}_{conv}$ obtained by relation (2) $\mathbf{k}_{inc}=\mathbf{k}_{A_1}$. (a) Rectangular grating and (b) square grating.

pulse generator delivers a very short pulse voltage (about 300 V for duration of 0.3 μs) to a piezocomposite transducer. The central frequency of this emitting transducer is 1 MHz and the −6 dB bandwidth is 660 kHz. Lamb waves are then generated by the wedge method. The surface displacements are detected by a laser interferometer. The interferometer remains unmoved whereas the plate with the emitter transducer is translated along the principal direction of the incident wave propagation. The interferometer collects the normal displacements from $x=10$ mm (origin $x=0$ corresponds to the wedge position) to $x=90$ mm by 0.1 mm step. For each position of the laser, a 100 μs long signal is stored with a 0.02 μs time step. In order to improve the signal to noise ratio, an average of 350 successive shots are performed. For each spatial position, the amplitude is recorded and then an (x, t) image is obtained as in the case of the finite element method (FEM) study. A 2D FFT is applied to the previous data: it gives the dispersion curves of the waves traveling in the plate in the (k, f) space. In Fig. 7 the amplitude of the incident waves are plotted versus frequencies. In the frequency-thickness range (2–4 MHz mm), the S_0 mode is

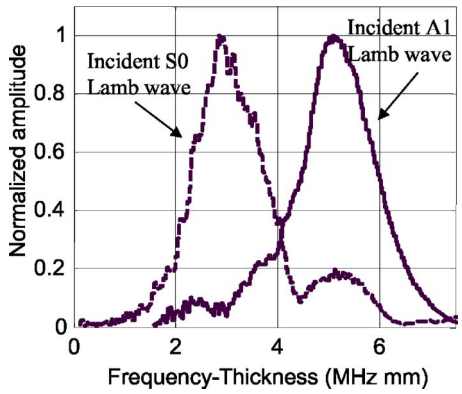

FIG. 7. Experimental study. Amplitude of the incident waves vs frequency-thickness product.

generated whereas the incident A_1 mode is present in the thickness-frequency range (4–6 MHz mm). The S_1 mode around its cutoff is also excited.

A. S_0 incident wave

Reflected signals in the wave number/frequency space are represented in Fig. 8 for a frequency range where the S_0 Lamb wave is incident. In the case of the rectangular profile, the converted A_1 and S_2 modes are reflected [respectively, spot (i) and (h) in Fig. 8(a)]. As in the FEM study these modes are linked to the second ($N=2$) harmonic of the grating. The conversion mode related to the S_1 incident mode is present: the reflected S_0 wave [spot (j)] related to the harmonic 2 of the grating $[k_{S_0}=k_{S_1}-2\pi/(\Lambda/2)]$. Figure 8(a) shows the S_0 standing wave [spot (k)] already observed in the FEM study [Fig. 4(a)]. The wavelength λ of this wave is equal to 4 mm corresponding to the difference between the period Λ and the length $a=2$ mm (see Fig. 1). Contrary to the case of the rectangular profile, the square profile has only odd harmonics. We verify that conversions (h) and (i) related to the harmonic 2 disappear [Fig. 4(b)]. Spots surrounded in dots are due to the S_1 incident mode. The A_0 reflected mode [spot (l)] is due to a conversion of the S_0 mode and verifies $k_{A_0}=k_{S_0}-2\pi/(\Lambda/3)$. The spot (m) is a standing S_0 wave with a wavelength $\lambda=3$ mm equal to the half of the square groove.

B. A_1 incident wave

In the frequency bandwidth where the A_1 wave is incident (Fig. 9), the converted waves (A_1, S_2, A_0/S_0) are also linked to the presence of the second and fourth harmonics in the PSD of the rectangular grating profile. The spot (n) is a reflected A_1 component of a standing wave with a wavenumber $k=2\pi/(\Lambda-a)=1570$ m^{-1}.

The 2D FFT on the square grating [Fig. 9(b)] exhibits converted waves due to the third harmonic. The A_0 reflected waves [spot (o)] at thickness-frequency $fe=5.25$ MHz mm results from the conversion of the S_1 reflected wave. Then, at this frequency three modes are coupled: A_1, S_1, and A_0 modes. The S_0 mode [spot (p)] and A_1 mode [spot (q)] are due to the presence of two standing waves with wave numbers $k=2\pi/(\Lambda-a)=2100$ m^{-1}.

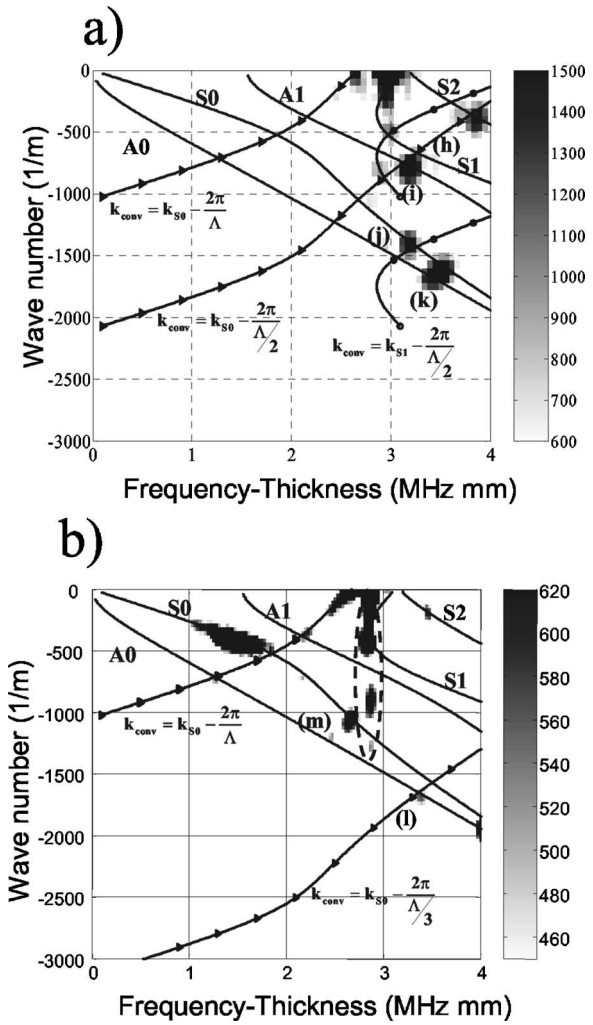

FIG. 8. Experimental study. Incident S_0 wave. Identification of the converted/reflected waves in the wavenumber/frequency space. The theoretical dispersion curves are plotted in solid line. The solid lines with triangle represent the wavenumbers $\mathbf{k}_{\text{conv}}$ obtained by relation (2) with $\mathbf{k}_{\text{inc}}=\mathbf{k}_{S_0}$. The solid lines with circle represent the wave numbers $\mathbf{k}_{\text{conv}}$ obtained by relation (2) with $\mathbf{k}_{\text{inc}}=\mathbf{k}_{S_1}$. (a) Rectangular grating and (b) square grating.

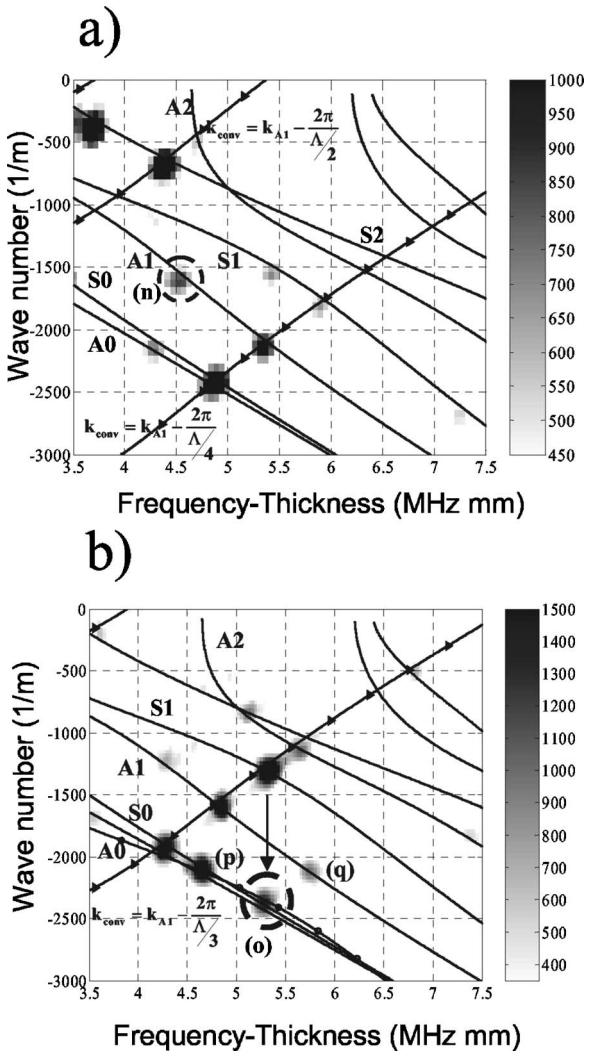

FIG. 9. Experimental study. Incident A_1 wave. Identification of the converted/reflected waves in the wave number/frequency space. The theoretical dispersion curves are plotted in solid line. The solid lines with triangle represent the wave numbers $\mathbf{k}_{\text{conv}}$ obtained by relation (2) with $\mathbf{k}_{\text{inc}}=\mathbf{k}_{S_0}$. The solid lines with a circle represent the wave numbers $\mathbf{k}_{\text{conv}}$ obtained by relation (2) with $\mathbf{k}_{\text{inc}}=\mathbf{k}_{S_1}$. (a) Rectangular grating and (b) square grating.

These results are consistent with those obtained by the FEM study. However, slight differences are observed between the frequencies of the converted waves in the experimental and the FEM studies. Indeed thicknesses of the experimental plates are slightly lower than the FEM plate model. Then there is a small shift of the wavenumbers of the Lamb wave. In the experiment the signal is a short pulse. The spectrum is only limited by the bandwidth of the broadband transducer. In the FEM the excitation is quasi harmonic and then the spectrum of the signal exhibits a low level for some frequencies. This fact explains why some conversions observed in experimental study are not observed in the FEM study. In spite of these small differences the two studies allow to conclude that a simple relationship exists between incident and converted wavevector and the surface grating profile. The wave vectors of the converted waves depend on the PSD of the grating profile. Some additional converted modes are also observed due to standing wave formed under surface grating.

It is well known[16] for a one-dimensional (1D) crystal that the propagating wave vector belongs to the first Brillouin zone. Here the grating can be considered as a 1D crystal. Therefore, it is convenient to study the coupling between Lamb modes insides the first Brillouin zone. This is the goal of the following section.

V. DISPERSION CURVES IN THE FIRST BRILLOUIN ZONE

In this section, the waveguide is considered as a repetition along the (Ox) direction of the elementary cell of the grating (Fig. 10). The finite element method consists in meshing only one unit cell of the grating and then using the

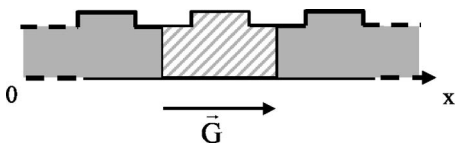

FIG. 10. Elementary periodic cell.

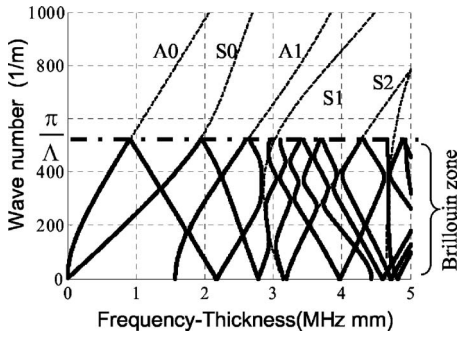

FIG. 11. Dispersion curves in the first Brillouin zone. Rectangular grating.

Bloch–Floquet relations,[17] which are the phase relations between nodes separated by one period. On each boundary of the pattern ($x=0$ and $x=\Lambda$), a Bloch–Floquet condition has to be fulfilled. The angular frequency ω is a periodic function of the wave vector $\mathbf{k}$ so the study becomes restricted to the first Brillouin zone. The dispersion diagram is plotted by varying the wave vector in a half Brillouin zone $[0;\ \pi/\Lambda]$ and then the other half zone $[-\pi/\Lambda;\ 0]$ is plotted symmetrically. The dispersion curves enable us to deduce propagation modes, cutoff frequencies, bandwidth, and stop bands.

In Fig. 11 the dispersion curves for the rectangular grating are plotted in the Brillouin zone. The periodicity of the guide implies that the Lamb waves dispersion curves fold back for $k=\pm\pi/\Lambda$ and $k=0$. The study of these dispersion curves shows the existence of gaps also called forbidden bands. These gaps are of two kinds: stop band at the limit of the Brillouin zone or "mini-stop band" into the Brillouin zone.[18]

Mini-stop bands are due to the opening of gap at the crossing of two Lamb mode dispersion curves. This leads to anti-crossing behavior of the dispersion curves. This case corresponds to mode coupling (mode conversion). Indeed, near the edge of the stop band, the group velocity vanishes and allows a possible conversion between two different modes. For the rectangular grating in Fig. 12, a mini-stop band appears at crossing between the S_0 and S_1 dispersion curves ($fe=3.85$ MHz *mm*). This implies an important band

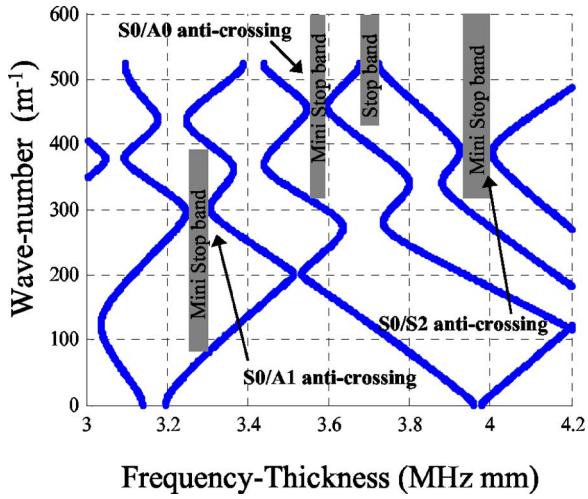

FIG. 12. Stop bands for the rectangular grating. Zoom of Fig. 11 in the range (3–4.2 MHz mm).

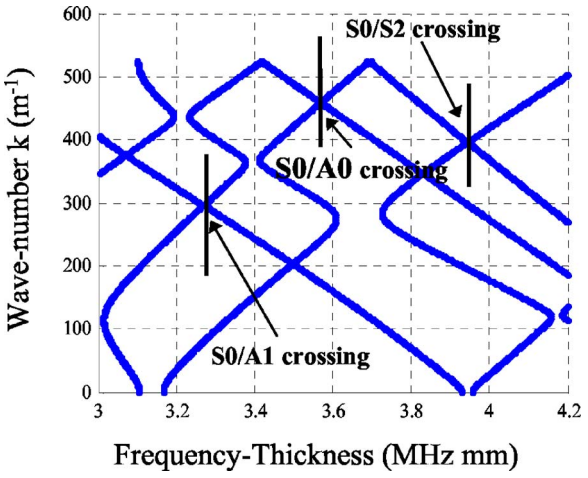

FIG. 13. Stop bands for the square grating.

gap and therefore a strong coupling between the mode S_0 and the mode S_2. Indeed a reflected mode S_2 is observed experimentally and by the FEM analysis in Fig. 4 [spot (a)] and Fig. 8(a) [spot (h)]. For the square grating in Fig. 13, the band gap is closed and the wave S_0 does not convert into the mode S_2 [Figs. 4(b) and 8(b)]. The same phenomenon is observed at the crossing of the S_0 and A_1 dispersion curves. A ministop band is present in Fig. 12 at $fe=3.25$ MHz *mm*. This forbidden band leads to a S_0 mode conversion in the A_1 mode. This conversion is observed in Fig. 4(a) [spot (b)] and Fig. 8(a) [spot (i)]. Stop bands seem to appear according to the grating period and implying the existence of an energy transfer between modes.

The second type of stop band exists at the boundary of the Brillouin zone. These stop bands are located in a frequency range where a dispersion curve folds back. An example of stop band is shown in Fig. 14 around the frequency-thickness product fe=3.7 MHz mm. This stop band is located at the limit $k=\pi/\Lambda$ where the S_0 dispersion curve is folding back. This point corresponds to the intersection of two dispersion branches shifted by $\pm m(2\pi/\Lambda)$ (m is an integer). This leads to relation (2) with $N=2$. This forbidden band is present for the square and the rectangular grating. In Figs. 4(a) and 4(b), reflections of the S_0 wave are observed around $fe=3.7$ MHz mm [spots (c) and (d)]. One can note that the amplitude of the S_0 reflected wave is stronger in the case of the rectangular grating and corresponds to a wider stop band.

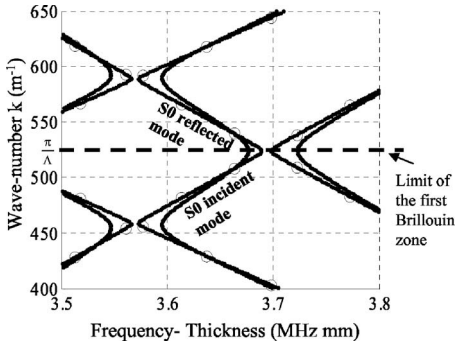

FIG. 14. Lamb wave dispersion curves for rectangular grating (solid lines) and square grating (solid lines with circles).

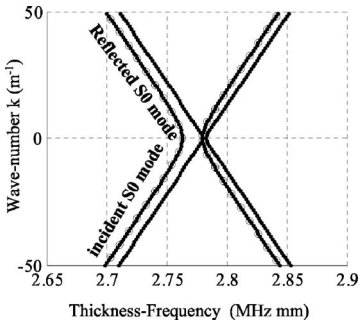

FIG. 15. Lamb wave dispersion curves for rectangular grating (solid lines) and square grating (solid lines with circles).

We also verify the link between opening of stop band and conversion phenomena for experimental results. Spot (m) is observed in Fig. 8(b) and corresponds to a reflected S_0 wave with a wave vector $\mathbf{k}=-1050\ \mathrm{m}^{-1}$. Figure 15 shows that a gap is open at this thickness-frequency product $fe=2.78$ MHz *mm* in the case of the square grating whereas the gap is closed for the rectangular one. At $k=0$ or $k=\pm\pi/\Lambda$, the opening of a stop band means that two counterpropagating modes are coupled.

VI. CONCLUSIONS

The process of mode conversions describes the interaction of Lamb wave with a periodic grating. This process is completely described in the dual space (wave number/frequency space). The spatial periods of the corrugated surface imply coupling between modes (conversions) and reflections. The coupling of modes is related to the opening of the band gaps in the fold-back dispersion curves in the first Brillouin zone. In this study the complex modes are not taken into account in the mode conversion process. In the future, it could be interesting to identify these localized modes. In particular, they are very important near a default of a grating as shown in the domain of photonic gratings.[18] As the opening of the stop band is strongly dependent on the PSD of the surface, further studies will treat this topic. This kind of study has not been developed in the crystal photonic field.

ACKNOWLEDGMENTS

This work is supported by the research group on ultrasonics (GDR CNRS No. 2501, France). The authors would like to thank Philippe Saint-Martin (I.U.T., Le Havre, France) for the machining of the experimental samples.

[1] O. I. Lobkis and D. E. Chimenti, J. Acoust. Soc. Am. **102**, 143 (1997).
[2] O. I. Lobkis and D. E. Chimenti, J. Acoust. Soc. Am. **102**, 150 (1997).
[3] D. Leduc, B. Morvan, P. Pareige, and J.-L. Izbicki, NDT Int. **37**, 207 (2004).
[4] C. Potel, D. Leduc, B. Morvan, P. Pareige, J.-L. Izbicki, and C. Depollier, Proceedings of the World Congress on Ultrasonics, Paris, France, 2003, Vol. 2, pp. 609–612.
[5] C. Potel, M. Bruneau, B. Morvan, J.-L. Izbicki, A.-C. Hladky-Hennion, and C. Depollier, Euro-African Workshop on Acoustics, Marrakech, December 2005.
[6] A. H. Nayfeh, J. Acoust. Soc. Am. **57**, 1036 (1975).
[7] J. C. Samuels, J. Acoust. Soc. Am. **31**, 319 (1959).
[8] S. E. Sandström, J. Acoust. Soc. Am. **79**, 1293 (1986).
[9] A. El-Bahrawy, J. Sound Vib. **170**, 145 (1994).
[10] S. Banerjee and T. Kundu, J. Acoust. Soc. Am. **119**, 2006 (2006).
[11] S. Banerjee and T. Kundu, Int. J. Solids Struct. **43**, 6551 (2006).
[12] T. Kundu and S. Banerjee, J. Acoust. Soc. Am. **120**, 1217 (2006).
[13] D. Leduc, A.-C. Hladky-Hennion, B. Morvan, J.-L. Izbicki, and P. Pareige, J. Acoust. Soc. Am. **118**, 2234 (2005).
[14] O. R. Asfar and A. H. Nayfeh, SIAM Rev. **25**, 455 (1983).
[15] ATILA Finite Element Code for Piezoelectric and Magnetostrictive Transducer Modeling, Version 5.2.1, User's Manual, ISEN, Acoustics Laboratory, Lille, France, 2002.
[16] L. Brillouin, *Wave Propagation in Periodic Structures* (Dover, New York, 1953).
[17] P. Langlet, A.-C. Hladky-Hennion, and J.-N. Decarpigny, J. Acoust. Soc. Am. **98**, 2792 (1995).
[18] J.-M. Lourtioz, *Les Cristaux Photoniques ou la Lumière en Cage* (Hermes-Lavoisier, Paris, 2003).